Mon. Not. R. Astron. Soc. **342,** 915–925 (2003)

9C: a survey of radio sources at 15 GHz with the Ryle Telescope

Elizabeth M. Waldram,★ Guy G. Pooley, Keith J. B. Grainge, Michael E. Jones, Richard D. E. Saunders, Paul F. Scott and Angela C. Taylor

Astrophysics Group, Cavendish Laboratory, Madingley Road, Cambridge CB3 0HE

Accepted 2003 March 2. Received 2003 February 19; in original form 2002 May 23

ABSTRACT

The fields chosen for the first observations of the cosmic microwave background with the Very Small Array have been surveyed with the Ryle Telescope at 15 GHz. We have covered three regions around RA $00^h\ 20^m$ Dec. $+30°$, RA $09^h\ 40^m$ Dec. $+32°$ and RA $15^h\ 40^m$ Dec. $+43°$ (J2000.0), an area of 520 deg^2. There are 465 sources above the current completeness limit of $\approx$25 mJy, although a total of $\approx$760 sources have been detected, some as faint as 10 mJy. This paper describes our techniques for observation and data analysis; it also includes source counts and some discussion of spectra and variability. Preliminary source lists are presented.

Key words: surveys – stars: individual: II Peg – cosmic microwave background – radio continuum: general.

1 INTRODUCTION

Foreground sources represent a major contaminant for centimetre-wave cosmic microwave background (CMB) measurements and our current survey with the Ryle Telescope at 15.2 GHz was set up as part of the observing strategy of the CMB telescope, the Very Small Array (VSA) (Watson et al. 2003). Its prime motivation has been to define a catalogue of the foreground sources that must be monitored by the VSA during its observations at a frequency of 34 GHz (Taylor et al. 2003). It is, however, of much wider interest, being the first survey covering an appreciable area at a radio frequency above the 4.8-GHz frequency of the Green Bank survey (Gregory et al. 1996). In particular, it provides a means of identifying gigahertz peaked spectrum (GPS) sources, which are important for the study of radio source evolution as well as being a significant foreground for CMB observations over a range of wavelengths. Since it will be a new, quite extensive survey, we have designated it '9C' or the ninth Cambridge survey.

The Ryle Telescope (RT) is an E–W radio synthesis telescope, the essential features of which are described by Jones (1991). The main problem in using the telescope for surveying the VSA fields is the small size of its primary beam envelope, which is only 6-arcmin FWHM, compared with 4.°6 for the VSA (for observations in its compact array). To overcome this, we have developed a new rastering technique which differs from the usual operation of the telescope in that we can cover a much wider area in a given time. A similar method was used to scan the foreground sources for the Cosmic Anisotropy Telescope (CAT) (Baker et al. 1999).

2 CHOICE OF FIELDS

The fields for the first CMB observations with the VSA were chosen to be as free as possible from contamination by Galactic or extragalactic foreground radiation, whether synchrotron, free–free or from dust. An attempt was made to select fields likely to contain no very bright radio sources (>0.5 Jy) at 30 GHz. To make this prediction, sources in the Green Bank 4.8-GHz survey were matched with those in the NVSS 1.4-GHz survey (Condon et al. 1998), and their 30-GHz flux densities calculated simply from their spectral indices based on these two frequencies. This was known to be unreliable but, in the absence of a higher-frequency survey, was the best indication available.

The first three areas were chosen to be more than 25° from the Galactic plane, spaced in RA and observable from both Tenerife (for the VSA) and Cambridge, UK (for the RT). They are in the regions around RA $00^h\ 20^m$ Dec. $+30°$, RA $09^h\ 40^m$ Dec. $+32°$ and RA $15^h\ 40^m$ Dec. $+43°$ (J2000.0). In each area a mosaic of overlapping VSA observations has been made and the RT survey is designed to cover the VSA primary beam out as far as a diameter of 9° for each pointing in the mosaic. In practice, we have covered significantly wider areas than the minimum required (see Section 6).

For more details of the criteria used in selecting the VSA fields see Taylor et al. (2003).

3 OBSERVATIONS AND DATA ANALYSIS

Since the area to be covered for each VSA pointing is 64 deg^2, while the area within the FWHM of the RT primary beam is only 0.01 deg^2, we have had to devise a technique whereby the RT survey can keep pace with the VSA observations. The principle of our method is to cover 1 deg^2 of sky in 12 h by making a raster scan of 240 different pointing directions during that time. We use the E–W array of five aerials spaced to give a resolution of 25 arcsec, or, in some configurations of the telescope, 12 arcsec. The 12 h of data are combined into a single map, which is used simply to identify peaks corresponding to possible radio sources. Each possible source

★E-mail: emw1@mrao.cam.ac.uk

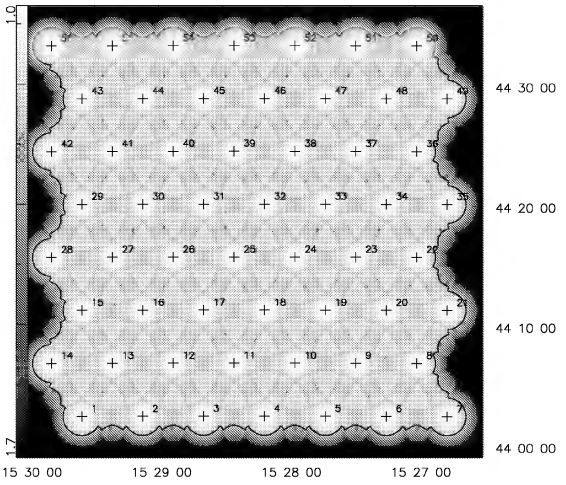

Figure 1. The sensitivity map corresponding to a 7 × 8 hexagonal array of pointing directions. The grey-scale shows the value of M_n (see Section 3.1). White indicates high sensitivity. (Here the coordinates are RA and Dec. B1950.0.)

is subsequently followed up with a short pointed observation of 10–15 min either to establish a reliable flux density or else to eliminate it as a false detection.

3.1 The rastering technique

The principle of our method is illustrated by one of our early trials. Fig. 1 shows a small raster of 56 pointing centres in a 7 × 8 hexagonal array, spaced at intervals of 5 arcmin. In this example, there are seven scans through the array during a 12-h observation, in the sequence shown, with a dwell time on each centre at each pass of 12 of the 8-s data samples. A phase calibrator is observed periodically during the run. We make 56 small maps (so-called 'component' maps), one for each pointing, and, at this stage, with no correction for the primary beam envelope. The uv aperture coverage is very sparse and is different for each map.

We calculate an appropriately weighted combination of the component maps to form a single large map with approximately uniform sensitivity (hereafter referred to as a 'raster' map). The map value M_r at any point on the raster map is derived from the individual map values (m_i) and primary beam values (p_i) of up to three overlapping component maps. We assume that each component map has the same noise value σ_c and add the map values corrected for the primary beam, (m_i/p_i), weighted by $(p_i/\sigma_c)^2$. This gives

$$M_r = \left(\sum_{i=1}^{i_{max}} m_i p_i\right)\left(\sum_{i=1}^{i_{max}} p_i^2\right)^{-1} \quad \text{where} \quad i_{max} = 1, 2 \text{ or } 3.$$

Only the region of each component map out as far as 0.3 of the primary beam maximum is used. We also calculate a second map in which the value M_n at the same point on the raster map is given by

$$M_n = \left(\sum_{i=1}^{i_{max}} p_i^2\right)^{-1/2} \quad \text{where} \quad i_{max} = 1, 2 \text{ or } 3.$$

M_n is essentially the inverse of the sensitivity at any point on a raster map (see Fig. 1). Thus, if in fact the noise values on the component maps were uniformly σ_c, the noise at any point on the raster map would be $M_n\sigma_c$. We have chosen the spacing of the component pointing centres (i.e. 5 arcmin) such that M_n varies only over a range from 1 to a maximum value of M_n^{max} within the main area of the raster map, where $M_n^{max} \approx 1.2$. M_n obviously rises steeply at the edges of the map and the contour in Fig. 1 indicates the area outside which it exceeds M_n^{max}.

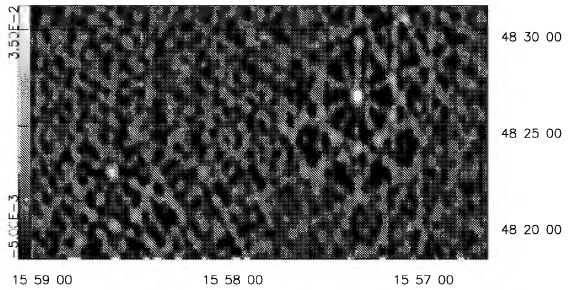

Figure 2. A section of a raster map with two sources of flux densities 50 and 36 mJy. (Here the coordinates are RA and Dec. B1950.0.)

Although with this configuration of 56 pointing centres we can reach noise levels of 1.5 mJy, the area of sky covered in 12 h is only 0.25 deg^2, and so in practice, for most of our observations, we use 240 pointing centres in a 15 × 16 hexagonal array, again spaced by 5 arcmin. There are then only five scans through the array during an observation, each with a theoretical dwell time of four of the 8-s data samples. The telescope pointing errors are monitored during the observations; for each baseline, those samples for which the mean pointing error of either aerial is excessive are excluded from the mapping process (we do not collect data during slewing). Consequently, one of the four 8-s data samples is usually lost. These larger raster maps cover an area of 1 deg^2 but the noise becomes about 4 mJy. Fig. 2 shows a section of such a map, with two sources of 50 and 36 mJy, and Fig. 3 shows the corresponding section of the sensitivity map.

The aperture coverage is extremely sparse for these 15 × 16 rasters, as can be seen from the 'spokes' in the source shapes. For example, the synthesized beam for the component map made from pointing centre 157 is shown in Fig. 4. However, our trials have shown that, since we are using the raster maps simply to locate peaks corresponding to possible sources, we can tolerate very sparse aperture coverage in order to maximize the speed of surveying.

Our method is similar to 'mosaicing' (Cornwell 1988; Sault et al. 1996) in that we are combining interferometric data from a series of pointing directions. However, mosaicing has traditionally been used to image extended objects that span several primary beams of the interferometer elements, whereas here we are only concerned to

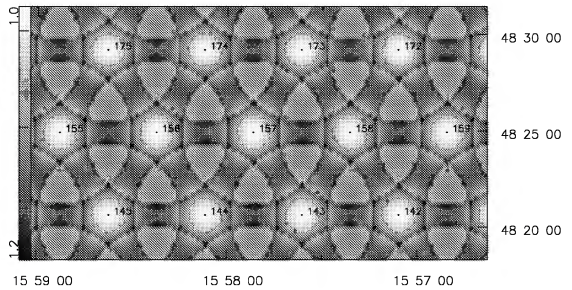

Figure 3. The section of the sensitivity map corresponding to the section of the raster map in Fig. 2. The numbers show the sequence of pointing centres. The grey-scale shows the value of M_n (see Section 3.1). White indicates high sensitivity.

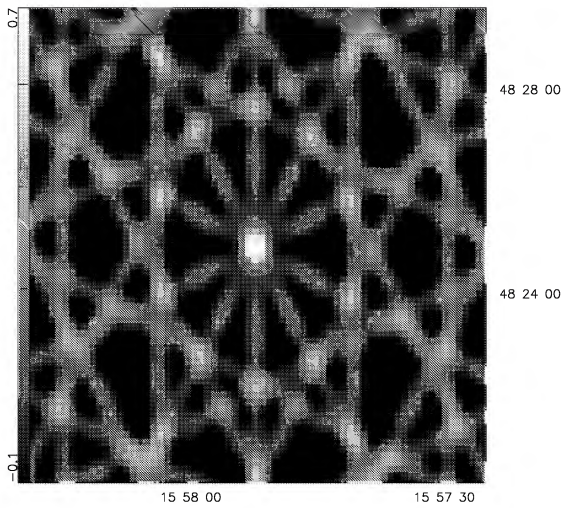

Figure 4. The synthesized beam for the component map corresponding to pointing centre 157 in Fig. 3. (Here the coordinates are RA and Dec. B1950.0.)

identify point sources. We do not attempt any joint deconvolution of the data, though we have shown that it is possible to apply CLEAN to the small component maps before combining them into a single raster map. We plan to CLEAN in the regions of very bright sources before publishing the final source catalogues, but this has not been undertaken for the preliminary lists presented here. For the purpose of the analysis in this paper we have excluded the source 4C39.25 (9.5 Jy) and the area around it; it does not lie within the regions selected for our preliminary lists (see Section 6).

3.2 Source extraction

Our source-finding method is constrained by the nature of the raster maps. Since the maps are not CLEANed, they include the effect of the strong sidelobes in the synthesized beam. Also, since different areas of the map are derived from different data, the noise may vary over the map, if there are varying weather conditions during the run. We therefore calculate both a mean noise value σ for the whole map and an estimate of the local noise at points corresponding to the pointing centres, to check for very noisy areas; if necessary the observation is repeated.

Since the sensitivity of the raster map falls steeply at the edges, it is possible to use the map of M_n to define the area within which we search for sources, i.e. we can search the area corresponding to that within the M_n^{max} contour. This has enabled us to use 'scalloped' rather than straight edges for our search area and so to position the raster maps as close together as possible. In our present method we scan this area of the raster map for local maximum pixels $\geqslant 3\sigma$. Since the maps are sufficiently sampled, we can then, for each maximum, calculate a peak value, corresponding to a position interpolated between the grid points. (This is done by calculating the local map values on a successively finer grid, by repeated convolution with an appropriate Gaussian-graded sinc function.) Peaks of height $\geqslant 5\sigma$ are selected to form a list of source candidates for subsequent pointed observations.

This source extraction technique was developed during the course of the survey analysis. In particular, the values of 3σ for the pixel cut-off and 5σ for the peak cut-off were chosen after a number of trials; we have aimed to find as many weak sources as possible without accumulating an excess of spurious responses. However, initially we simply extracted from the raster maps the positions of local maximum pixels $\geqslant 5\sigma$, and an area of $\sim$100 deg^2 out of the total 520 deg^2 has been processed in this way. To assess the effect on the catalogue, we have made a comparison of the results from our old and new algorithms over an area of $\sim$40 deg^2. We find only eight sources that were missed by the earlier method; all of these are below our estimated completeness limit of 25 mJy. Our conclusion is that, since we already have varying sensitivity over the whole survey area, the effect of the change in the procedure is minimal.

Pointed observations are made for each source candidate. A total observing time of about 15 min (much longer than the observing time for any one patch of the raster field) is sufficient to give a clear confirmation, or otherwise. By observing a group of nearby candidates in sequence, we spread this 15 min over 2 or 3 h of hour angle and therefore are able to make useful maps to search for any extended sources; some 6 per cent are resolved in this way. We estimate that the flux densities have uncertainties of 5 per cent or less.

We find that the measured flux densities from the pointed observations are systematically higher (by about 10 per cent) than the estimates based on the raster maps. This has no significant consequence for the source list, since the rasters are simply used to locate the sources. The difference in scales is probably a result of the compromise necessary between keeping as much data as possible and discarding that with excessive pointing errors (see Section 3.1).

4 COMPLETENESS

The layout of the observations is arranged to have small overlaps between the raster maps to ensure complete coverage of the required area. However, since the noise varies from raster map to raster map, as well as within the maps, there is some variation in sensitivity over the survey. We have investigated the completeness in two ways.

The first method has been to plot the ratio, S_r/S_p, of raster flux density to pointed flux density versus S_p, as in Fig. 5. It can be seen that, although for the brighter sources there is the expected scatter, below 25 mJy the ratio rises significantly. Our conclusion is that for these weaker sources the only peaks that are detected on the raster maps are those boosted by a positive local noise contribution, and that this implies a completeness limit of $\approx$25 mJy.

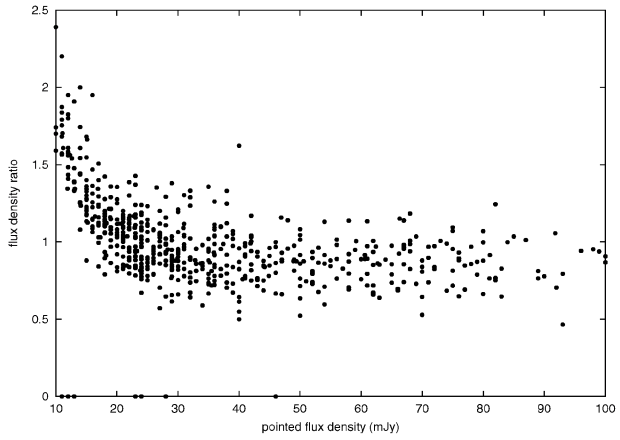

Figure 5. Plot of the ratio (S_r/S_p) of raster flux density to pointed flux density versus S_p. (Where the ratio is shown as zero, the corresponding source lies in an area of a raster map that is hard to interpret. A pointed observation has been made but there is no definitive raster flux density.)

Secondly, we have made a deeper survey of a smaller area of 15 deg^2, within the area of the main survey, using mostly 9×8 raster scans. A 12-h observation then covers an area of only 0.25 deg^2 but the noise level on a raster map becomes $\approx$1.8 mJy and a plot such as that in Fig. 5 indicates that the completeness limit becomes $\approx$10 mJy. A comparison of the source count for the deeper area with that for the main area confirms our estimate of $\approx$25 mJy as the completeness limit of the main survey. It is not possible at present to be more precise concerning this completeness limit, since the deeper count includes too few sources, i.e. a total of only 68, with only seven above 25 mJy. However, the indication is that at lower flux densities the completeness of the main survey is much reduced, falling to $\approx$10 per cent at the 10-mJy level.

5 SOME PROPERTIES OF THE SURVEY

5.1 Source count

Fig. 6 shows the differential source counts. It demonstrates the completeness limits, from the turnovers in the counts, at $\approx$25 mJy for the main survey and at $\approx$10 mJy for the deeper survey. For comparison, we have included the 1.4-GHz NVSS differential count, as calculated from the sources in that catalogue in our survey areas.

Fig. 7 shows the normalized differential counts $S^{5/2}n(S)$, i.e. our counts divided by the counts expected in a Euclidean universe. Points considered to be affected by incompleteness have been omitted; these include the point in the main survey corresponding to the 25–30 mJy bin, which may be marginally affected as our completeness estimate is only approximate. We also show a count from an earlier survey at 15 GHz that we made over an area of 17 deg^2 during the source scanning for the CAT observations. This was in a completely different area of the sky from the current survey region. However, the deeper survey described here was made over an area

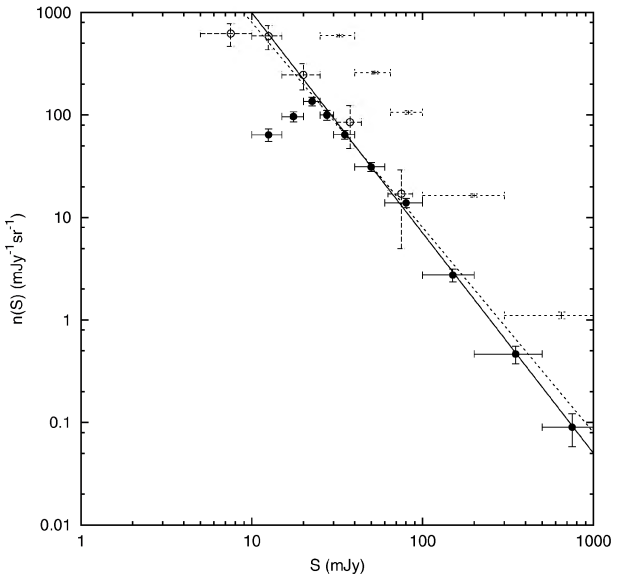

Figure 6. Plot of the differential source count for both the main survey (filled circles) and the deeper survey (open circles). The third count is the NVSS 1.4-GHz count, as calculated from our survey areas. The horizontal bars show the bin widths and the vertical bars show the random errors. The solid line is the function we have fitted to the main count. The function from the earlier paper (Taylor et al. 2001) has been added (dashed) for comparison. (See Section 5.1.)

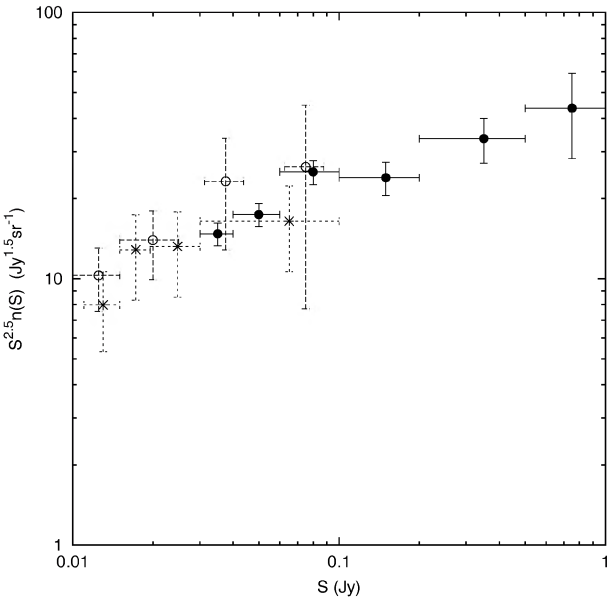

Figure 7. Plot of the normalized differential source count for both the main survey (filled circles) and the deeper survey (open circles). The third count (stars) is from an earlier survey at 15 GHz, made for the CAT observations.

within the main survey and therefore the two contain some sources in common.

We have calculated a least-squares fit of the function AS^b to the differential count of the main survey, using the data in Table 1, with weights appropriate to the Poisson errors $\sqrt{N}$ in N, and find

$$n(S) \equiv \frac{\mathrm{d}N}{\mathrm{d}S} \approx 51 \left(\frac{S}{\mathrm{Jy}}\right)^{-2.15} \mathrm{Jy}^{-1}\,\mathrm{sr}^{-1}.$$

The effect of random errors in the flux densities is to produce an overestimate of the value of N in each bin. However, in our case this is negligible, since the 5 per cent uncertainty would cause only a $\sim$0.75 per cent increase. We have, however, made a correction for the bin widths. We take S to be the value at the centre of a bin and multiply the corresponding N by a factor of $(1 - r^2)$, where $r = W/2S$. Here we are making the approximation that $n(S) \propto S^{-2}$ within any bin but are making no assumption concerning the size of the bin.

The survey is entirely limited by noise, and not by source confusion. At 10 mJy, there are some 7200 sources per steradian, or 6×10^6 arcsec^2 per source. The beamwidth of the observations described here, 25×25 cosec δ arcsec^2, means that there are typically 5000 beam areas per source, far above the value at which early radio

Table 1. Table showing the data used in fitting the source count for the main survey. The area is 0.1584 sr. S is the flux density at the centre of the bin. We assume Poisson errors $\sqrt{N}$ in N.

Bin centre S/Jy	Width of bin W/Jy	Number in bin N
0.0350	0.010	104
0.0500	0.020	103
0.0800	0.040	94
0.1500	0.100	49
0.3500	0.300	27
0.7500	0.500	8

source counts suffered from 'confusion'. Since the pointed observations are used to make adequate maps of each source, there is very seldom any problem in deciding whether a multiple source is really that or a chance coincidence.

Our fitted function is consistent with the data presented in the earlier source count paper (Taylor et al. 2001) but should provide a more accurate representation of the count, since it is based on a much larger sample of sources. The function quoted in that paper has been added to Fig. 6 for comparison.

5.2 Correlation with NVSS at 1.4 GHz

We have correlated our source lists with the catalogue from the 1.4-GHz NVSS survey, which has a similar resolution to ours (see Fig. 8). All the sources in the main survey in this paper have counterparts in NVSS, apart from two, one of which has been found in the deeper 1.4-GHz FIRST survey (Becker, White & Helfand 1995), leaving only one hitherto uncatalogued source. The horizontal line in Fig. 8 marks the estimated completeness limit of 25 mJy; there are 465 sources above this limit.

A histogram of the spectral index distribution $\alpha_{1.4}^{15.2}$ for the 465 sources above the survey limit of 25 mJy is shown in Fig. 9, where α is defined by $S \propto \nu^{-\alpha}$. Of these sources, 88 (19 per cent) have inverted spectra, i.e. $\alpha_{1.4}^{15.2} < 0$. However, the distribution of spectral index for the 84 sources $\geqslant$100 mJy (shaded in Fig. 9) appears to be significantly different, with 26 (31 per cent) having $\alpha_{1.4}^{15.2} < 0$.

Our correlation with NVSS shows the importance of the new survey in the investigation of the source population at high frequencies. This can be illustrated by considering all the sources $\geqslant$25 mJy in NVSS within our areas, 4089 sources in all. A possible procedure might have been to make pointed observations of all these sources at 15 GHz, in which case we should have found 434 sources above our survey limit of 25 mJy. However, 31 sources above our limit (i.e. 6.7 per cent of the total) would have been missed, since their flux densities in NVSS are <25 mJy.

Our correlation can also give some indication of the proportion of sources in the NVSS catalogue with inverted spectra; this is important for any attempt to predict the source population at high frequencies from that at 1.4 GHz. Out of the 4089 sources $\geqslant$25 mJy in NVSS in our areas, we find 57, above our survey limit of 25 mJy, to have $\alpha_{1.4}^{15.2} < 0$, i.e. 1.4 per cent have rising spectra between 1.4 and 15.2 GHz. We clearly cannot plot the complete spectral index distribution for the 4089 sources but the distribution of these negative spectral indices is shown in Fig. 10. This cannot, of course,

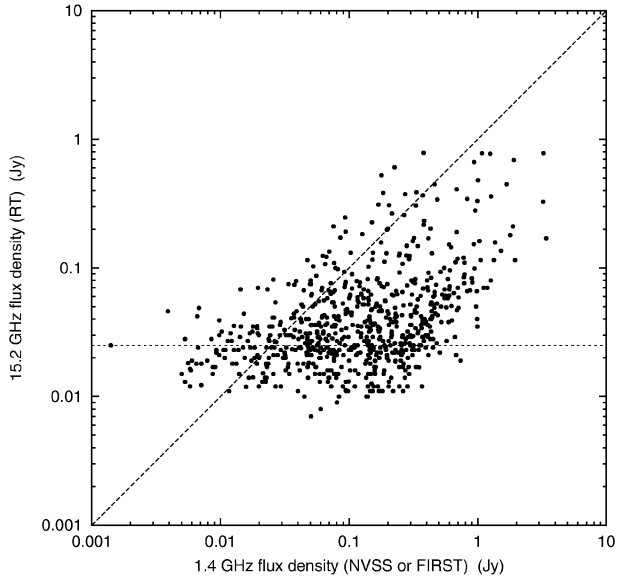

Figure 8. Plot of RT 15.2-GHz pointed flux densities (in the main survey) versus NVSS (or FIRST) 1.4-GHz flux densities, with a line indicating zero spectral index. The horizontal line is the estimated completeness limit.

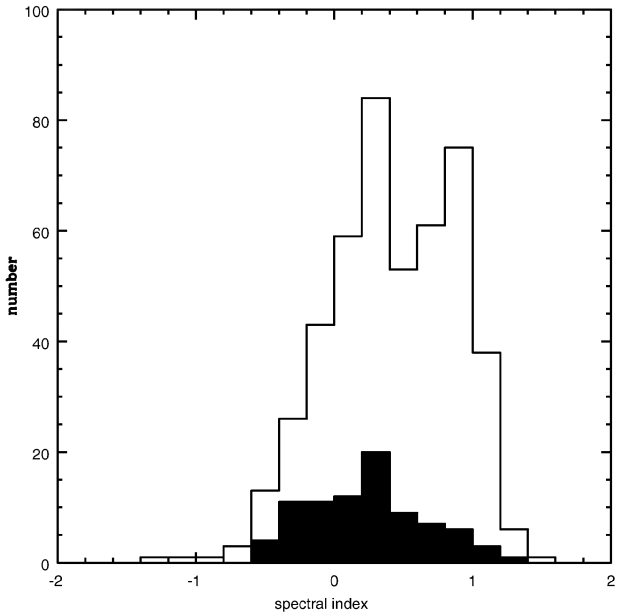

Figure 9. Histogram (unshaded) of the spectral index distribution $\alpha_{1.4}^{15.2}$ for the 465 sources $\geqslant$25 mJy in our survey, where α is defined by $S \propto \nu^{-\alpha}$. The shaded histogram shows the spectral index distribution for the 84 sources $\geqslant$100 mJy.

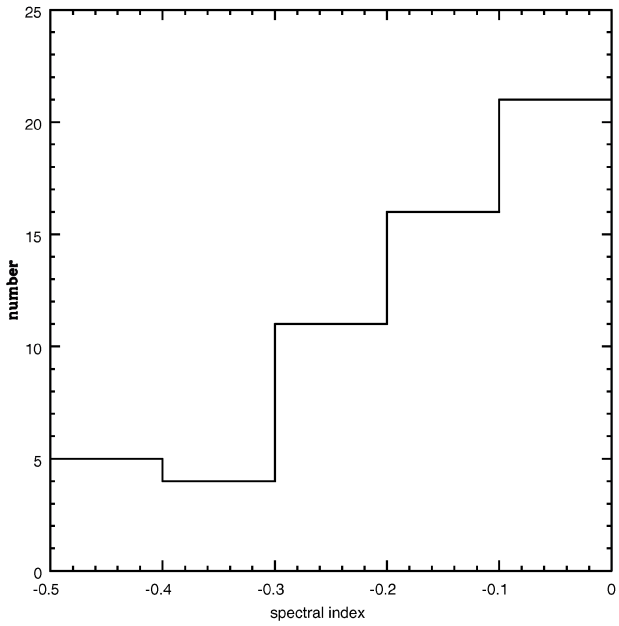

Figure 10. Histogram of the spectral index distribution $\alpha_{1.4}^{15.2}$ for the sources $\geqslant$25 mJy in both our survey and NVSS, with $\alpha < 0$.

provide information concerning inverted spectrum sources <25 mJy in NVSS, though we can see from Fig. 9 that some do have more extreme negative spectral indices.

We should emphasize that the observations at 1.4 and 15.2 GHz are not simultaneous and many of the sources are likely to be highly variable.

5.3 Variability

We have made a preliminary check on variability by re-observing a sample of all sources above 60 mJy in an area of 94 deg^2. The time intervals were between 1 and 14 months. Out of the 35 sources, eight were found to have varied by more than 20 per cent and, of these, one by more than 30 per cent and one by more than 60 per cent. Examples of two highly variable sources, used as phase calibrators in our survey, are shown in Figs 11 and 12. The estimated uncertainties in the flux densities are $\leqslant$5 per cent.

We have also identified the highly variable RS CVn star II Pegasi (van den Oord & de Bruyn 1994), which lies within our survey area (see Fig. 13). As in the detection by van den Oord & de Bruyn, we were alerted by the variation in flux density during the mapping observation. (This source has been excluded from the source lists used in this paper.)

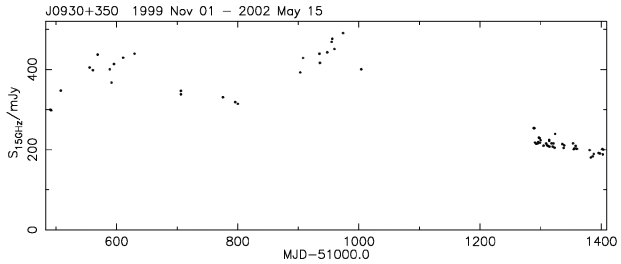

Figure 11. The variable source J0930+350: 1999 November to 2002 May.

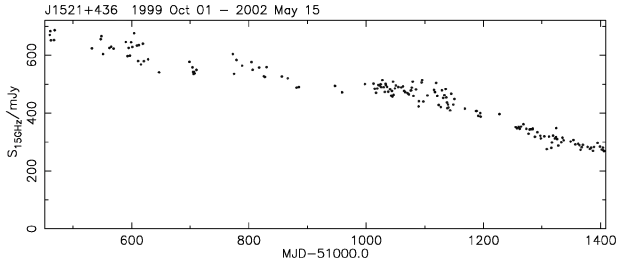

Figure 12. The variable source J1521+436: 1999 October to 2002 May.

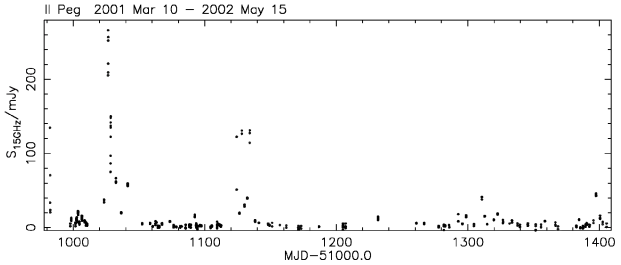

Figure 13. The variable RS CVn star II Pegasi: 2001 March to 2002 May.

6 PRELIMINARY SOURCE LISTS

6.1 Sky coverage

This is an on-going survey and, as explained earlier, its primary aim has been to cover the fields of the VSA observations, each of which contains a mosaic of pointing directions. This means that the regions of sky corresponding to our current source lists are necessarily ragged in shape and difficult to specify concisely. We have been working on extending the survey to form more easily defined regions and shall publish these in due course. For the purpose of this paper, in order to be able to define the areas simply and precisely, we have selected three circular areas, designated VSA1, VSA2, VSA3 (see Table 2), and present the source lists corresponding to these.

6.2 Description of the lists

We have included in these lists only those sources with flux densities above our estimated completeness limit of 25 mJy (see Section 4), a total of 242 sources. The definitions of the entries are shown in Table 3. The source lists are in Tables 4–6.

The position of a source is derived from the raster map, unless the follow-up pointed observation indicates a significant difference, in which case that position is substituted. We have checked the positions of a sample of 19 sources, which appear on two raster maps and estimate that our position accuracy is better than 10 arcsec. For bright sources, the accuracy is better than 3 arcsec, as determined from the observations of the 17 sources in our VSA2 list, all brighter than 60 mJy at 15 GHz, which are found in the Jodrell VLA calibrator survey (Wilkinson et al. 1998, and references therein).

Our flux densities are those from the pointed observations. The uncertainty in these is dominated by the random uncertainty in the flux calibration, which we estimate to be ~5 per cent. Since many of the sources are highly variable, we also quote the date of the pointed observation.

6.3 Availability of the catalogues

These lists are available via our web page http://www.mrao.cam.ac.uk/surveys/index.html. They are preliminary lists only and will be extended and refined as the survey proceeds. The web page will be updated accordingly.

Table 2. The circular areas corresponding to the source lists.

	Centre J2000 RA (^{h} ^{m} ^{s}) Dec. ($^\circ$ $'$ $''$)	Centre B1950 RA (^{h} ^{m} ^{s}) Dec. ($^\circ$ $'$ $''$)	Radius (deg)	Area (deg^2)
VSA1	00 17 36.5 30 16 39	00 15 00.0 30 00 00	5.5	95.0
VSA2	09 40 57.7 31 46 21	09 38 00.0 32 00 00	6.0	113.0
VSA3	15 36 42.7 43 20 11	15 35 00.0 43 30 00	5.0	78.5

Table 3. Definitions of the entries in the source lists.

Column	Description	Example
1	Source name	9CJ0002+3032
2	J2000 RA ^{hms}	00 02 49.2
3	J2000 Dec. $^\circ$ $'$ $''$	30 32 43
4	B1950 RA ^{hms}	00 00 15.2
5	B1950 Dec. $^\circ$ $'$ $''$	30 16 01
6	Flux density Jy	0.046
7	Date yymmdd	000531

Table 4. Source list for the VSA1 field.

Source name	RA J2000	Dec. J2000	RA B1950	Dec. B1950	Flux density (Jy)	Date
9CJ0000+2914	00 00 35.2	29 14 28	23 58 01.5	28 57 47	0.036	010119
9CJ0002+3139	00 02 14.2	31 39 42	23 59 40.2	31 23 00	0.036	000622
9CJ0002+3032	00 02 49.2	30 32 43	00 00 15.2	30 16 01	0.046	000531
9CJ0002+2942	00 02 52.4	29 42 55	00 00 18.4	29 26 13	0.052	000819
9CJ0003+2740	00 03 13.0	27 40 46	00 00 39.0	27 24 04	0.075	000619
9CJ0003+3010	00 03 55.6	30 10 02	00 01 21.3	29 53 20	0.081	000531
9CJ0003+3241	00 03 56.3	32 41 54	00 01 22.0	32 25 12	0.065	000622
9CJ0004+2637	00 04 23.7	26 37 52	00 01 49.5	26 21 10	0.071	000531
9CJ0004+2946	00 04 34.6	29 46 17	00 02 00.2	29 29 35	0.067	000531
9CJ0005+3206	00 05 40.4	32 06 06	00 03 05.9	31 49 25	0.096	000622
9CJ0005+3139	00 05 55.8	31 39 49	00 03 21.2	31 23 07	0.076	000622
9CJ0006+3422	00 06 07.3	34 22 19	00 03 32.6	34 05 38	0.075	000622
9CJ0006+2523	00 06 28.5	25 23 01	00 03 54.0	25 06 19	0.050	001107
9CJ0010+3403	00 10 03.8	34 03 12	00 07 28.3	33 46 31	0.029	000321
9CJ0010+2838	00 10 11.1	28 38 11	00 07 35.9	28 21 30	0.061	000904
9CJ0010+2854	00 10 27.8	28 54 58	00 07 52.5	28 38 16	0.038	000904
9CJ0010+2717	00 10 28.7	27 17 54	00 07 53.6	27 01 13	0.036	000405
9CJ0010+2619	00 10 36.3	26 19 19	00 08 01.2	26 02 38	0.065	000405
9CJ0010+2956	00 10 42.5	29 56 12	00 08 07.1	29 39 31	0.061	000325
9CJ0010+2650	00 10 51.3	26 50 28	00 08 16.1	26 33 47	0.036	000405
9CJ0011+3443	00 11 17.3	34 43 34	00 08 41.5	34 26 53	0.029	001011
9CJ0011+2803	00 11 34.2	28 03 48	00 08 58.8	27 47 07	0.039	000405
9CJ0011+2928	00 11 46.0	29 28 30	00 09 10.5	29 11 49	0.053	000325
9CJ0012+2702	00 12 38.2	27 02 40	00 10 02.7	26 45 59	0.072	000816
9CJ0012+3353	00 12 47.3	33 53 36	00 10 11.3	33 36 55	0.098	000221
9CJ0013+2834	00 13 32.7	28 34 53	00 10 57.0	28 18 12	0.028	000108
9CJ0013+3441	00 13 44.1	34 41 41	00 11 07.8	34 25 01	0.136	001005
9CJ0013+2646	00 13 46.5	26 46 42	00 11 10.9	26 30 02	0.030	000816
9CJ0014+2815	00 14 33.8	28 15 07	00 11 58.0	27 58 27	0.048	000108
9CJ0015+3216	00 15 06.2	32 16 13	00 12 29.9	31 59 33	0.448	000107
9CJ0015+3052	00 15 36.1	30 52 24	00 12 59.9	30 35 44	0.035	000108
9CJ0016+2510	00 16 39.8	25 10 28	00 14 04.0	24 53 49	0.052	000816
9CJ0018+2921	00 18 12.5	29 21 24	00 15 35.9	29 04 45	0.084	000109
9CJ0019+2817	00 19 08.9	28 17 56	00 16 32.3	28 01 17	0.035	000001
9CJ0019+2956	00 19 37.8	29 56 02	00 17 01.0	29 39 23	0.043	000109
9CJ0019+2602	00 19 39.8	26 02 52	00 17 03.4	25 46 14	0.409	000816
9CJ0019+2647	00 19 52.5	26 47 31	00 17 16.0	26 30 52	0.053	000531
9CJ0019+3320	00 19 58.6	33 20 02	00 17 21.3	33 03 24	0.036	000110
9CJ0020+3152	00 20 50.6	31 52 30	00 18 13.3	31 35 51	0.041	000109
9CJ0021+2711	00 21 28.7	27 11 44	00 18 52.0	26 55 05	0.039	000221
9CJ0021+3226	00 21 29.9	32 26 57	00 18 52.5	32 10 19	0.027	000109
9CJ0022+3250	00 22 43.8	32 50 46	00 20 06.0	32 34 09	0.025	000110
9CJ0023+3114	00 23 10.0	31 14 01	00 20 32.4	30 57 24	0.033	000110
9CJ0023+2734	00 23 14.5	27 34 30	00 20 37.4	27 17 52	0.067	000221
9CJ0023+2539	00 23 23.1	25 39 19	00 20 46.2	25 22 42	0.124	001006
9CJ0024+2510	00 24 16.0	25 10 38	00 21 39.1	24 54 01	0.047	001006
9CJ0026+3508	00 26 41.7	35 08 42	00 24 02.8	34 52 07	0.152	000911
9CJ0027+2830	00 27 00.6	28 30 23	00 24 22.8	28 13 47	0.026	000110
9CJ0027+2607	00 27 27.0	26 07 08	00 24 49.5	25 50 33	0.032	000601
9CJ0027+2555	00 27 29.6	25 55 32	00 24 52.2	25 38 57	0.052	001006
9CJ0028+3103	00 28 10.8	31 03 50	00 25 32.4	30 47 15	0.027	000303
9CJ0028+2914	00 28 17.1	29 14 29	00 25 39.0	28 57 54	0.089	991127
9CJ0028+2954	00 28 31.9	29 54 52	00 25 53.6	29 38 17	0.030	001006
9CJ0029+3456	00 29 14.3	34 56 34	00 26 34.9	34 39 59	0.689	001007
9CJ0029+3244	00 29 33.0	32 44 52	00 26 54.0	32 28 17	0.047	000305
9CJ0030+2957	00 30 05.3	29 57 07	00 27 26.8	29 40 33	0.032	991127
9CJ0030+3415	00 30 21.5	34 15 58	00 27 42.0	33 59 24	0.029	000305
9CJ0030+2833	00 30 28.7	28 33 37	00 27 50.4	28 17 04	0.049	000110
9CJ0030+2809	00 30 57.1	28 09 43	00 28 18.8	27 53 10	0.030	000110
9CJ0031+3016	00 31 21.9	30 16 04	00 28 43.1	29 59 31	0.056	000303
9CJ0032+2758	00 32 44.6	27 58 56	00 30 06.0	27 42 24	0.038	000222
9CJ0033+2752	00 33 09.7	27 52 30	00 30 31.1	27 35 58	0.026	000308
9CJ0034+2754	00 34 43.5	27 54 26	00 32 04.6	27 37 54	0.344	000303
9CJ0036+3151	00 36 48.1	31 51 14	00 34 07.9	31 34 44	0.080	000309
9CJ0036+2958	00 36 59.8	29 58 58	00 34 20.1	29 42 28	0.122	000305
9CJ0037+3002	00 37 10.2	30 02 44	00 34 30.4	29 46 14	0.034	000817

Table 4 – *continued*

Source name	RA J2000	Dec. J2000	RA B1950	Dec. B1950	Flux density (Jy)	Date
9CJ0038+2932	00 38 31.4	29 32 19	00 35 51.5	29 15 50	0.030	000305
9CJ0039+3114	00 39 08.4	31 14 21	00 36 28.0	30 57 52	0.026	000610
9CJ0041+3211	00 41 16.0	32 11 08	00 38 35.0	31 54 41	0.170	000604
9CJ0042+3005	00 42 39.8	30 05 59	00 39 59.2	29 49 34	0.029	000604
9CJ2352+3030	23 52 54.7	30 30 24	23 50 22.3	30 13 43	0.036	010130
9CJ2353+3040	23 53 06.7	30 40 49	23 50 34.3	30 24 08	0.037	010130
9CJ2353+3136	23 53 19.5	31 36 18	23 50 47.2	31 19 37	0.079	010131
9CJ2353+2931	23 53 58.6	29 31 04	23 51 26.0	29 14 23	0.035	010329
9CJ2354+2758	23 54 48.4	27 58 31	23 52 15.6	27 41 49	0.029	010315
9CJ2355+3032	23 55 03.2	30 32 51	23 52 30.5	30 16 09	0.027	010130
9CJ2355+3150	23 55 20.6	31 50 41	23 52 47.9	31 33 59	0.035	010131
9CJ2355+2835	23 55 54.1	28 35 55	23 53 21.2	28 19 14	0.118	010329
9CJ2357+2747	23 57 36.0	27 47 21	23 55 02.8	27 30 39	0.041	010119
9CJ2358+3129	23 58 13.7	31 29 58	23 55 40.4	31 13 16	0.029	010209
9CJ2358+2754	23 58 34.2	27 54 09	23 56 00.9	27 37 27	0.064	010119
9CJ2358+2936	23 58 47.7	29 36 09	23 56 14.3	29 19 27	0.036	010131
9CJ2359+2703	23 59 00.2	27 03 25	23 56 26.8	26 46 43	0.042	010315
9CJ2359+3021	23 59 19.5	30 21 04	23 56 46.1	30 04 22	0.030	010124

Table 5. Source list for the VSA2 field.

Source name	RA J2000	Dec. J2000	RA B1950	Dec. B1950	Flux density (Jy)	Date
9CJ0915+2933	09 15 52.5	29 33 21	09 12 53.6	29 45 52	0.148	000816
9CJ0917+3446	09 17 16.2	34 46 36	09 14 11.8	34 59 11	0.067	001225
9CJ0919+3324	09 19 08.8	33 24 42	09 16 06.2	33 37 23	0.524	000307
9CJ0920+3312	09 20 21.0	33 12 39	09 17 18.9	33 25 23	0.058	000307
9CJ0920+2755	09 20 27.5	27 55 52	09 17 30.8	28 08 37	0.052	000212
9CJ0921+2834	09 21 52.9	28 34 53	09 18 55.7	28 47 42	0.057	000107
9CJ0922+3232	09 22 26.0	32 32 26	09 19 24.9	32 45 16	0.025	000213
9CJ0923+3107	09 23 48.0	31 07 56	09 20 48.5	31 20 50	0.148	000220
9CJ0923+2815	09 23 51.6	28 15 26	09 20 54.9	28 28 20	0.374	000107
9CJ0925+3026	09 25 25.3	30 26 35	09 22 26.7	30 39 33	0.025	000218
9CJ0925+3159	09 25 32.8	31 59 54	09 22 32.6	32 12 53	0.068	000213
9CJ0925+3626	09 25 39.2	36 26 30	09 22 34.3	36 39 29	0.040	010220
9CJ0925+3127	09 25 43.6	31 27 12	09 22 44.1	31 40 11	0.232	000220
9CJ0925+3612	09 25 51.9	36 12 38	09 22 47.3	36 25 37	0.265	001108
9CJ0926+2758	09 26 45.2	27 58 22	09 23 49.2	28 11 24	0.062	000108
9CJ0926+2711	09 26 59.4	27 11 06	09 24 04.1	27 24 09	0.030	000307
9CJ0927+2954	09 27 22.5	29 54 13	09 24 24.7	30 07 17	0.029	991127
9CJ0927+3034	09 27 39.8	30 34 16	09 24 41.4	30 47 20	0.063	991127
9CJ0927+2738	09 27 56.0	27 38 18	09 25 00.4	27 51 23	0.026	000220
9CJ0928+2904	09 28 15.0	29 04 16	09 25 18.2	29 17 22	0.027	991127
9CJ0930+3601	09 30 33.7	36 01 15	09 27 30.1	36 14 27	0.210	000611
9CJ0930+3503	09 30 55.3	35 03 38	09 27 52.8	35 16 51	0.340	000611
9CJ0931+2734	09 31 01.9	27 34 50	09 28 06.8	27 48 04	0.035	000307
9CJ0931+2750	09 31 51.8	27 50 52	09 28 56.5	28 04 08	0.087	000213
9CJ0932+2837	09 32 14.3	28 37 31	09 29 18.3	28 50 48	0.058	000819
9CJ0932+3339	09 32 55.1	33 39 29	09 29 54.3	33 52 48	0.124	000106
9CJ0933+2845	09 33 37.4	28 45 32	09 30 41.5	28 58 52	0.036	991127
9CJ0933+3254	09 33 39.7	32 54 42	09 30 39.9	33 08 02	0.029	000108
9CJ0934+2756	09 34 20.5	27 56 04	09 31 25.4	28 09 26	0.028	000215
9CJ0934+3050	09 34 47.3	30 50 57	09 31 49.6	31 04 21	0.045	991127
9CJ0935+3633	09 35 31.8	36 33 18	09 32 28.5	36 46 44	0.149	001008
9CJ0935+2917	09 35 36.2	29 17 11	09 32 40.1	29 30 37	0.036	991127
9CJ0936+3207	09 36 03.8	32 07 14	09 33 05.1	32 20 40	0.041	991127
9CJ0936+2554	09 36 06.7	25 54 10	09 33 13.6	26 07 37	0.029	001105
9CJ0936+3313	09 36 09.4	33 13 09	09 33 09.7	33 26 36	0.037	000106
9CJ0936+2624	09 36 14.2	26 24 04	09 33 20.7	26 37 31	0.063	001105
9CJ0937+3206	09 37 06.4	32 06 56	09 34 07.8	32 20 25	0.059	000106
9CJ0937+3411	09 37 16.5	34 11 33	09 34 15.9	34 25 03	0.062	000221
9CJ0938+2611	09 38 20.6	26 11 33	09 35 27.5	26 25 06	0.031	001110
9CJ0938+2559	09 38 54.7	25 59 40	09 36 01.8	26 13 15	0.037	001114
9CJ0939+2908	09 39 01.6	29 08 29	09 36 06.1	29 22 04	0.109	000222
9CJ0939+3556	09 39 49.9	35 56 14	09 36 48.0	36 09 51	0.115	000531

Table 5 – *continued*

Source name	RA J2000	Dec. J2000	RA B1950	Dec. B1950	Flux density (Jy)	Date
9CJ0940+2626	09 40 13.5	26 26 57	09 37 20.4	26 40 35	0.062	001105
9CJ0940+2547	09 40 14.5	25 47 10	09 37 22.0	26 00 48	0.032	001110
9CJ0940+2603	09 40 14.7	26 03 30	09 37 22.0	26 17 07	0.448	001114
9CJ0940+3015	09 40 18.8	30 15 09	09 37 22.5	30 28 46	0.066	000106
9CJ0941+2547	09 41 42.9	25 47 22	09 38 50.6	26 01 04	0.030	001110
9CJ0941+2728	09 41 48.1	27 28 38	09 38 54.4	27 42 20	0.158	000222
9CJ0941+2722	09 41 52.4	27 22 18	09 38 58.7	27 36 00	0.045	000221
9CJ0942+3309	09 42 15.3	33 09 30	09 39 16.6	33 23 13	0.061	000107
9CJ0942+2626	09 42 31.2	26 26 57	09 39 38.4	26 40 40	0.038	001105
9CJ0942+3344	09 42 36.2	33 44 38	09 39 36.9	33 58 21	0.054	000326
9CJ0942+3737	09 42 54.8	37 37 36	09 39 51.7	37 51 20	0.039	001008
9CJ0943+2833	09 43 02.1	28 33 57	09 40 07.6	28 47 41	0.025	001011
9CJ0943+3614	09 43 19.1	36 14 52	09 40 17.5	36 28 37	0.210	001011
9CJ0943+3300	09 43 33.5	33 00 14	09 40 35.0	33 14 00	0.041	000222
9CJ0944+3347	09 44 20.2	33 47 56	09 41 21.1	34 01 44	0.039	000222
9CJ0944+2554	09 44 42.3	25 54 42	09 41 50.2	26 08 30	0.120	001201
9CJ0945+2729	09 45 15.6	27 29 11	09 42 22.3	27 43 01	0.092	000308
9CJ0945+3656	09 45 23.1	36 56 02	09 42 21.1	37 09 52	0.029	000831
9CJ0945+2640	09 45 31.0	26 40 54	09 42 38.3	26 54 44	0.082	000308
9CJ0945+3534	09 45 38.2	35 34 58	09 42 37.6	35 48 48	0.305	000821
9CJ0945+2755	09 45 56.7	27 55 56	09 43 03.1	28 09 47	0.044	000222
9CJ0946+3309	09 46 10.9	33 09 05	09 43 12.8	33 22 57	0.025	000222
9CJ0948+3423	09 48 38.6	34 23 17	09 45 39.7	34 37 15	0.051	000326
9CJ0949+2711	09 49 10.9	27 11 13	09 46 18.4	27 25 12	0.053	000408
9CJ0949+2921	09 49 24.2	29 21 41	09 46 29.9	29 35 41	0.029	000222
9CJ0949+2920	09 49 48.2	29 20 53	09 46 53.9	29 34 54	0.071	000222
9CJ0949+3626	09 49 53.0	36 26 18	09 46 52.4	36 40 19	0.042	001010
9CJ0950+2743	09 50 33.7	27 43 28	09 47 40.9	27 57 31	0.038	000222
9CJ0951+3451	09 51 11.5	34 51 33	09 48 12.6	35 05 37	0.034	000603
9CJ0951+3359	09 51 45.7	33 59 33	09 48 47.7	34 13 39	0.028	000603
9CJ0952+2828	09 52 06.1	28 28 32	09 49 12.9	28 42 38	0.158	000222
9CJ0952+3606	09 52 26.5	36 06 01	09 49 26.6	36 20 09	0.048	001010
9CJ0952+3512	09 52 32.0	35 12 52	09 49 33.0	35 26 59	0.388	001010
9CJ0953+3225	09 53 28.0	32 25 52	09 50 31.7	32 40 02	0.102	000222
9CJ0954+3456	09 54 06.7	34 56 45	09 51 08.2	35 10 56	0.046	000603
9CJ0954+3335	09 54 26.8	33 35 22	09 51 29.6	33 49 33	0.037	000109
9CJ0954+3019	09 54 27.6	30 19 10	09 51 33.2	30 33 22	0.032	000222
9CJ0954+2639	09 54 39.8	26 39 24	09 51 48.3	26 53 36	0.162	000324
9CJ0955+3335	09 55 37.9	33 35 04	09 52 40.9	33 49 18	0.075	000408
9CJ0955+3533	09 55 47.7	35 33 24	09 52 49.0	35 47 39	0.038	001225
9CJ0956+3032	09 56 37.7	30 32 41	09 53 43.4	30 46 58	0.030	000317
9CJ0956+2855	09 56 40.7	28 55 46	09 53 47.7	29 10 03	0.030	000324
9CJ0957+3422	09 57 46.4	34 22 16	09 54 49.1	34 36 36	0.062	000818
9CJ0957+3150	09 57 51.1	31 50 46	09 54 56.0	32 05 06	0.040	000901
9CJ0958+3224	09 58 20.9	32 24 03	09 55 25.4	32 38 23	0.774	000818
9CJ0958+3307	09 58 27.0	33 07 28	09 55 30.8	33 21 49	0.033	000408
9CJ0958+2948	09 58 58.9	29 48 04	09 56 05.6	30 02 26	0.076	000317
9CJ1000+2752	10 00 07.6	27 52 46	09 57 15.9	28 07 10	0.082	001015
9CJ1000+3437	10 00 27.4	34 37 40	09 57 30.3	34 52 06	0.026	000824
9CJ1000+2752	10 00 29.4	27 52 12	09 57 37.8	28 06 37	0.071	001015
9CJ1001+2911	10 01 10.2	29 11 39	09 58 17.6	29 26 06	0.198	000818
9CJ1001+3424	10 01 11.9	34 24 50	09 58 15.2	34 39 17	0.306	000825
9CJ1001+2846	10 01 46.3	28 46 55	09 58 54.1	29 01 23	0.170	000818
9CJ1002+3042	10 02 33.0	30 42 08	09 59 39.5	30 56 38	0.043	000824
9CJ1003+2845	10 03 13.5	28 45 26	10 00 21.6	28 59 57	0.093	000818
9CJ1003+3347	10 03 26.8	33 47 29	10 00 30.9	34 02 01	0.068	000828
9CJ1003+3244	10 03 57.6	32 44 03	10 01 02.6	32 58 36	0.202	000824
9CJ1004+3010	10 04 11.6	30 10 33	10 01 18.8	30 25 07	0.046	001107
9CJ1004+3151	10 04 32.9	31 51 53	10 01 38.8	32 06 27	0.080	000824
9CJ1006+3236	10 06 07.7	32 36 28	10 03 13.2	32 51 05	0.074	010208
9CJ1007+3003	10 07 14.9	30 03 52	10 04 22.5	30 18 32	0.079	010131

Table 6. Source list for the VSA3 field.

Source name	RA J2000	Dec. J2000	RA B1950	Dec. B1950	Flux density (Jy)	Date
9CJ1510+4221	15 10 17.9	42 21 54	15 08 29.0	42 33 13	0.065	000622
9CJ1511+4430	15 11 42.7	44 30 45	15 09 57.7	44 41 59	0.060	000815
9CJ1512+4540	15 12 27.1	45 40 26	15 10 44.2	45 51 37	0.030	000622
9CJ1513+4554	15 13 50.7	45 54 23	15 12 08.5	46 05 30	0.038	000622
9CJ1516+4349	15 16 31.5	43 49 49	15 14 46.2	44 00 48	0.027	000816
9CJ1516+4159	15 16 59.6	41 59 34	15 15 11.3	42 10 31	0.044	001106
9CJ1518+4618	15 18 44.7	46 18 56	15 17 04.2	46 29 46	0.054	000816
9CJ1518+4131	15 18 47.2	41 31 36	15 16 58.6	41 42 27	0.040	001108
9CJ1519+4254	15 19 27.0	42 54 08	15 17 40.7	43 04 57	0.047	000816
9CJ1520+4211	15 20 39.7	42 11 13	15 18 52.4	42 21 57	0.082	001106
9CJ1521+4336	15 21 49.6	43 36 39	15 20 04.9	43 47 20	0.605	000816
9CJ1523+4156	15 23 09.3	41 56 25	15 21 22.1	42 07 02	0.061	000301
9CJ1525+4201	15 25 23.6	42 01 18	15 23 36.9	42 11 46	0.052	000301
9CJ1526+4201	15 26 45.4	42 01 42	15 24 58.8	42 12 06	0.070	000301
9CJ1528+4219	15 28 00.2	42 19 14	15 26 14.3	42 29 34	0.046	000316
9CJ1528+4233	15 28 19.9	42 33 36	15 26 34.5	42 43 54	0.032	000301
9CJ1528+4522	15 28 41.1	45 22 16	15 27 00.8	45 32 33	0.046	000222
9CJ1529+4538	15 29 10.4	45 38 22	15 27 30.7	45 48 38	0.029	000223
9CJ1529+3945	15 29 49.8	39 45 10	15 28 00.1	39 55 24	0.036	010126
9CJ1531+4356	15 31 02.6	43 56 38	15 29 20.1	44 06 47	0.031	000222
9CJ1531+4048	15 31 40.9	40 48 26	15 29 53.1	40 58 34	0.040	000316
9CJ1532+4604	15 32 50.7	46 04 47	15 31 12.5	46 14 50	0.062	000222
9CJ1533+4107	15 33 27.9	41 07 23	15 31 40.9	41 17 24	0.030	000316
9CJ1533+3934	15 33 44.3	39 34 20	15 31 54.9	39 44 20	0.032	010126
9CJ1534+3834	15 34 50.5	38 34 10	15 32 59.7	38 44 06	0.026	010402
9CJ1536+3833	15 36 13.8	38 33 28	15 34 23.2	38 43 19	0.183	010402
9CJ1536+4627	15 36 17.3	46 27 33	15 34 40.4	46 37 23	0.037	000223
9CJ1536+3845	15 36 23.2	38 45 52	15 34 32.9	38 55 43	0.107	010402
9CJ1538+4225	15 38 55.8	42 25 27	15 37 11.8	42 35 09	0.055	000223
9CJ1539+4217	15 39 25.6	42 17 27	15 37 41.6	42 27 07	0.031	000223
9CJ1539+4735	15 39 34.8	47 35 31	15 38 00.9	47 45 10	0.191	000604
9CJ1539+4602	15 39 35.1	46 02 49	15 37 58.1	46 12 28	0.027	000223
9CJ1540+4138	15 40 43.0	41 38 18	15 38 58.0	41 47 53	0.030	000223
9CJ1541+4114	15 41 01.3	41 14 28	15 39 15.6	41 24 02	0.035	000604
9CJ1541+4456	15 41 10.2	44 56 31	15 39 31.3	45 06 05	0.035	000223
9CJ1541+4727	15 41 44.3	47 27 51	15 40 10.5	47 37 22	0.027	000823
9CJ1542+4359	15 42 22.8	43 59 13	15 40 42.2	44 08 42	0.027	000820
9CJ1545+4751	15 45 08.6	47 51 55	15 43 36.2	48 01 13	0.190	000820
9CJ1545+4130	15 45 21.4	41 30 27	15 43 36.8	41 39 46	0.058	000817
9CJ1545+4622	15 45 25.5	46 22 45	15 43 50.1	46 32 03	0.026	000823
9CJ1546+4257	15 46 22.6	42 57 57	15 44 40.7	43 07 11	0.038	000817
9CJ1547+4208	15 47 59.0	42 08 53	15 46 16.0	42 18 01	0.076	000824
9CJ1548+4031	15 48 11.3	40 31 27	15 46 25.5	40 40 35	0.070	000824
9CJ1550+4536	15 50 43.8	45 36 24	15 49 07.7	45 45 23	0.031	000825
9CJ1550+4545	15 50 54.8	45 45 28	15 49 19.0	45 54 25	0.027	000825
9CJ1553+4039	15 53 15.6	40 39 27	15 51 30.6	40 48 16	0.036	001118
9CJ1554+4350	15 54 15.7	43 50 29	15 52 36.6	43 59 14	0.036	010629
9CJ1554+4348	15 54 42.3	43 48 19	15 53 03.3	43 57 03	0.042	000828
9CJ1556+4257	15 56 36.2	42 57 07	15 54 55.8	43 05 44	0.115	000827
9CJ1556+4259	15 56 57.7	42 59 42	15 55 17.4	43 08 18	0.056	000827
9CJ1557+4522	15 57 19.0	45 22 21	15 55 43.4	45 30 55	0.145	001118
9CJ1558+4146	15 58 24.1	41 46 36	15 56 41.8	41 55 06	0.029	000827
9CJ1559+4349	15 59 31.3	43 49 16	15 57 53.0	43 57 42	0.059	000828
9CJ1601+4123	16 01 27.9	41 23 51	15 59 45.3	41 32 09	0.066	010621
9CJ1601+4316	16 01 40.5	43 16 48	16 00 01.5	43 25 06	0.042	001117

7 CONCLUSIONS AND FURTHER WORK

Our rastering technique with the Ryle Telescope has been used successfully to produce the first section of the 9C survey at 15 GHz; hitherto there has been no comparable high-frequency radio survey of any extent. Although it has been designed specifically for use with the centimetre-wave CMB observations of the Very Small Array, our survey has much wider implications. We have explored several of its properties: the source count, the correlation with the NVSS 1.4-GHz survey and the variability of the sources. These are important in studies of the radio source population at high frequencies, as well as in predicting the contaminating effect of foreground sources on CMB observations over a range of wavelengths.

The completeness limit of the main part of the survey described here is ≈25 mJy, but we are currently surveying further areas at the deeper level in order to provide appropriate source lists for the latest VSA observations, which are being made with its extended array at an increased sensitivity. These areas of the survey should reach a completeness limit of ≈10 mJy.

ACKNOWLEDGMENTS

We are grateful to the staff of our observatory for the operation of the Ryle Telescope, which is funded by PPARC. ACT acknowledges a PPARC studentship.

REFERENCES

Baker J.C. et al., 1999, MNRAS, 308, 1173
Becker R.H., White R.L., Helfand D.J., 1995, ApJ, 450, 559
Condon J.J., Cotton W.D., Greisen E.W., Yin Q.F., Perley R.A., Taylor G.B., Broderick J.J., 1998, AJ, 115, 1693
Cornwell T.J., 1988, A&A, 202, 316
Gregory P.C., Scott W.K., Douglas K., Condon J.J., 1996, ApJS, 103, 427
Jones M.E., 1991, in Cornwell T.J., Perley R., eds, ASP Conf. Ser. Vol. 19, Radio Interferometry – Theory, Techniques and Applications. Astron. Soc. Pac., San Francisco, p. 395
Sault R.J., Staveley-Smith L., Brouw W.N., 1996, A&AS, 120, 375
Taylor A.C., Grainge K.J.B., Jones M.E., Pooley G.G., Saunders R.D.E., Waldram E.M., 2001, MNRAS, 327, L1-L4
Taylor A.C. et al., 2003, MNRAS, 341, 1066
van den Oord G.H.J., de Bruyn A.G., 1994, A&A, 286, 181
Watson R.A. et al., 2003, MNRAS, 341, 1057
Wilkinson P.N., Browne I.W.A., Patnaik A.R., Wrobel J.M., Sorathia B., 1998, MNRAS, 300, 790

This paper has been typeset from a TEX/LATEX file prepared by the author.